Orbital-Occupancy versus Charge Ordering and the Strength of Electron Correlations in Electron-Doped $CaMnO_3$

Weidong Luo,[1,2] Alberto Franceschetti,[1,2] Maria Varela,[2] Jing Tao,[2] Stephen J. Pennycook,[2] and Sokrates T. Pantelides[1,2]

[1]*Department of Physics and Astronomy, Vanderbilt University, Nashville, Tennessee 37235, USA*

[2]*Materials Science and Technology Division, Oak Ridge National Laboratory, Oak Ridge, Tennessee 37831, USA*

(Received 12 October 2006; published 19 July 2007)

The structural, electronic, and magnetic properties of mixed-valence compounds are believed to be governed by strong electron correlations. Here we report benchmark density-functional calculations in the spin-polarized generalized-gradient approximation (GGA) for the ground-state properties of doped $CaMnO_3$. We find excellent agreement with all available data, while inclusion of strong correlations in the GGA + U scheme impairs this agreement. We demonstrate that formal oxidation states reflect only orbital occupancies, not charge transfer, and resolve outstanding controversies about charge ordering.

DOI: 10.1103/PhysRevLett.99.036402 PACS numbers: 71.15.Mb, 71.27.+a, 75.10.−b, 75.47.Lx

In mixed-valence compounds, a transition-metal (TM) element such as Mn would have a fractional ''valence'' or ''formal oxidation state'' unless one distinguishes two species of different integral oxidation states. Examples are the manganites ($R_xA_{1-x}MnO_3$, where R is a trivalent and A is a divalent ion, e.g., La and Ca, respectively), where the nominal Mn valence is $4 - x$. These materials exhibit complex behavior, including colossal magnetoresistance, phase separation, and spatial ordering of two inequivalent Mn atoms [1–5]. This spatial ordering occurs typically for $x \leq 0.5$. It is attributed to Mn^{+3} and Mn^{+4} oxidation states and is generally interpreted as charge ordering. This phenomenon and accompanying structural distortions and magnetic ordering are widely believed to be manifestations of strong electron correlations. In recent years, however, the presence of physical-charge ordering has been challenged [6–10].

Density-functional theory (DFT) [11,12] is generally viewed as inadequate for transition-metal oxides. Alternative theories such as the local spin-density approximation augmented by a Hubbard U (LSDA + U) [13], GGA + U, and dynamical mean-field theory (DMFT) [14] that include local correlations in the form of a ''Hubbard U'' are viewed as more suitable alternatives [15–19].

DFT is a ground-state theory. Ground-state properties constitute the real test of the applicability of DFT to mixed-valence compounds. A careful examination of the literature, however, reveals a lack of systematic tests of DFT predictions of ground-state properties to establish benchmarks for discrepancies to be addressed by theories that incorporate additional electron correlations. In this Letter, we report such systematic tests for $R_xCa_{1-x}MnO_3$ for x from 0 to 0.5 and establish the following: the predicted structural, electronic, and magnetic ground-state properties are in excellent agreement with all available data for $R =$ La and $R =$ Bi, obviating strong electron correlations. In addition, inclusion of strong local correlations by the GGA + U scheme impairs the agreement with the data. The generality of these results is discussed in the context of available data and calculations of ground-state properties for other mixed-valence compounds and in the context of theories for energy gaps.

The $La_xCa_{1-x}MnO_3$ (LCMO) system has been widely studied by experiments and theory. Experimental studies of $Bi_xCa_{1-x}MnO_3$ (BCMO) were recently reported by some of the present coauthors [20]. Electron-energy loss spectra (EELS) demonstrated that the structural ordering of inequivalent Mn atoms is accompanied by ordering of their ''formal oxidation states,'' as extracted from L_{23} ratios (the ratios of the areas under the initial peak of the L_2 and L_3 spectra) [20]. At first glance, this direct evidence of oxidation-state ordering adds further to the controversy as it appears to contradict the data that find no charge ordering [6,7,9]. The theoretical results to be presented here resolve the apparent conflict and elucidate the underlying physics.

Density-functional calculations were performed using spin-polarized generalized-gradient approximation (GGA) and the projector augmented-wave (PAW) method as implemented in the VASP code [21,22]. Convergence tests for k points and energy cutoff were performed to ensure numerical accuracy. For doped CMO, the calculations were based on ''generic doping'' by introducing extra electrons compensated by a uniform positive background (the approximation is justified by the experimental fact that the dopants are randomly distributed [20]). Calculations using real dopants should in principle be done in large supercells with different dopant arrangements followed by averaging over such arrangements. Such an undertaking is not practical. However, for 50% doping, we performed calculations for ordered $La_{0.5}Ca_{0.5}MnO_3$, which confirmed the validity of generic doping. Atomic-orbital occupancies were obtained from the eigenvalues of the on-site density matrix as implemented in the VASP code based on the PAW approach [21,22]. For GGA + U calculations, the results of which are reported at the end of the Letter, we also used the VASP implementation with U = 8.0 eV on the Mn $3d$ orbitals

(U = 7.9 eV was calculated for Pr-doped CMO [18]; U = 8.0 eV was used for $LaMnO_3$ in Ref. [23]) and U = 5.0 eV (used in a model Hamiltonian for La-doped CMO [16]).

The DFT/GGA results for ground-state properties are as follows:

Structure.—For undoped CMO, the predicted lowest-energy structure is *Pnma*, as observed. Theoretical lattice constants agree with experimental values to better than 1%. For 33% doping, tripling the *Pnma* cell in the [100] direction led to a lower-energy structure, as observed in both La-doped [24] and Bi-doped CMO with ABB ordering of Mn atoms. Tripling the *Pnma* cell in the [101] direction led to a secondary phase, also with ABB ordering, matching the phase reported in Ref. [20]. For 50%-doped CMO, doubling the *Pnma* cell in the [100] direction led to a lower-energy $P2_1/m$ structure, as observed in La-doped CMO [3] with AB ordering of Mn atoms. Inequivalent Mn atoms are characterized by their differences in local Jahn-Teller distortions (the calculated bond lengths are within 2% of measured values).

Electronic properties.—Calculated valence-band densities of states (DOS) of the CMO system at 0, 33%, and 50% doping are in excellent agreement with photoemission data, as shown in Fig. 1.

Magnetic ordering.—The total energy differences between ferromagnetic (FM) and antiferromagnetic (AF) orderings as a function of doping are plotted in Fig. 2. Results are given for both generic doping and, in the case of 50% doping, for ordered-La doping. Because the theoretical supercell volume for generic doping is not the same as the volume of the La-doped systems, we present results for both experimentally observed volumes and theoretical volumes. Agreement with the observed magnetic ordering is excellent; the theoretical value for transition from AF to FM ordering is 0.4–0.45, compared with the experimental value of 0.52.

Given the good agreement between theory and available experimental data on ground-state properties, we now use the theoretical results to resolve outstanding conflicts about charge and oxidation-state ordering, which are ground-state properties that are not measured directly, but are inferred from relevant data.

In Fig. 3(a), we show projected DOS (PDOS) for the two inequivalent Mn atoms in 50%-doped CMO and compare them with the PDOS of pure Mn metal. This and similar plots for other manganites establish a correspondence between the PDOS, which reflects orbital occupancies, and formal oxidation states, e.g., Mn^0 in Mn metal and nominally Mn^{+3} and Mn^{+4} for the two inequivalent Mn in doped CMO. This correlation underlies the observed connection between the L_{23} ratios extracted from EELS and formal oxidation state [2,20]. More detailed evidence for the relation between orbital occupancy and the formal oxidation state is presented below.

Physical charge on each Mn atom is a different matter. Charge is usually calculated by integrating the electron density in a specified volume (sphere or other shape), but depends sensitively on the choice of volume [25]. Alternatively, charge is calculated by adding occupancies of atom-centered basis functions, as in Mulliken population analysis [26], which attributes electron density in a cation's core region to nearby anions and vice versa. We avoid these ambiguities by plotting the integrated electron density within a sphere around a Mn atom as a function of the radius, as in Fig. 3(b). It is clear that, despite very different orbital occupancies, the net spherically averaged

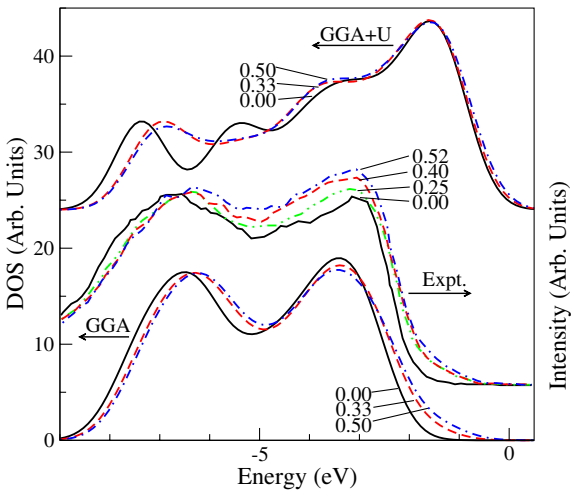

FIG. 1 (color online). Valence-band DOS of electron-doped CMO obtained using GGA and GGA + U (U = 8.0 eV), compared with photoemission data from Ref. [35] (the calculated DOS has been broadened with a Gaussian function, and the zero energy point at different dopings are adjusted).

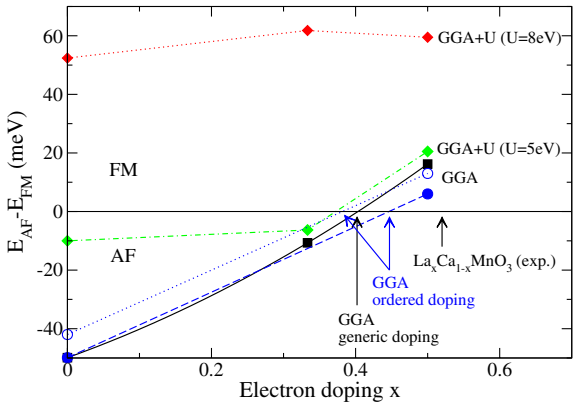

FIG. 2 (color online). Total energy difference between the AF and FM phases in generically doped $CaMnO_3$ (black squares) and in chemically ordered $La_{0.5}Ca_{0.5}MnO_3$ [blue (or dark gray) circles], as obtained using GGA. For generic doping, the experimental $La_xCa_{1-x}MnO_3$ cell volumes were used. Solid (open) symbols correspond to experimental (theoretical) volumes. Also shown are the results from GGA + U calculations (diamonds). The lines are guide to the eye. The arrows indicate the doping at which a AF/FM transition occurs in the two GGA calculations and in experiments.

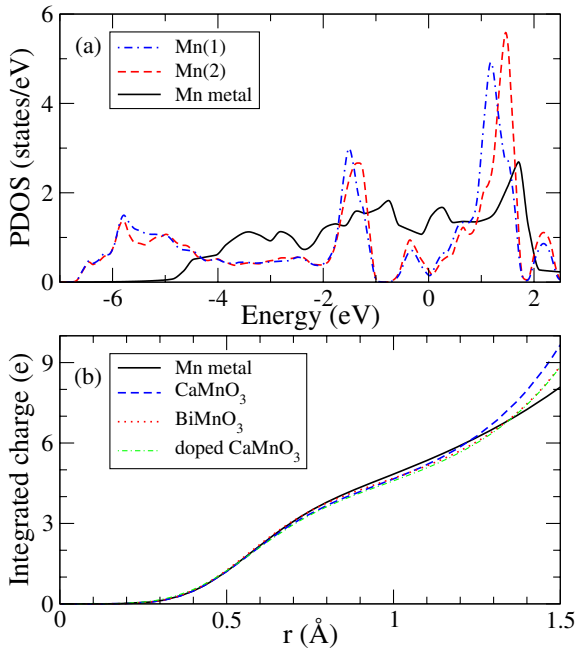

FIG. 3 (color online). (a) PDOS for the Mn 3*d* orbital of the two inequivalent Mn atoms [Mn(1) and Mn(2)] in 50%-doped CMO and the corresponding 3*d* PDOS in Mn metal. The Fermi energy is at $E_F = 0$. (b) The integrated valence electron density within a sphere around Mn atoms in Mn metal and several Mn oxides as a function of the radius of the integration sphere.

physical charges associated with Mn atoms in different oxides are essentially the same as in the metal; i.e., all atoms are practically neutral. The results shown in Fig. 3(b) are consistent with prior theoretical findings: the charge on the transition-metal atom is always found to be essentially the same on inequivalent sites (inclusion of strong correlations—see below—does not alter the result) [2]. The only difference is that, by choosing a particular integration radius or other way to define a precise value of charge, most authors typically report a value of +2.

Orbital occupancies can be defined by projecting Bloch functions on atomiclike orbitals. We calculated the on-site occupancies of the majority-spin Mn 3*d* orbitals (eigenvalues of the on-site density matrix) using the PAW scheme [22] for the entire family of Mn oxides and found that they exhibit a pattern that correlates with formal oxidation states, shown in Table I. Even though the occupancies do not exactly correspond to formal oxidation states, the correlation between the columns in bold in Table I is sufficient to account for the observed dependence of L_{23} ratios on oxidation state. We note that the orbital-occupancy results reflect ordering of the local Mn magnetic moments as well. From GGA calculations of the 33% and 50%-doped AF phase CMO, inequivalent Mn atoms have different spin density and magnetic moments, which reflect different orbital occupancies, while the integrated charges are practically the same.

The overall conclusion is that the doping of CMO leads to diverse low-symmetry structures with two distinct Mn local geometries. The resulting crystal wave functions have distinct orbital occupancies at the two sites. These occupancies correlate with the formal oxidation states because the sum of cation oxidation states must be equal to the number of electrons needed to fill the O 2*p* bands [2]. The concept is useful because the O 2*p* bands are always low in energy and completely full. These bands, however, are hybridized with TM-atom orbitals so that their filling does not entail charge transfer [2]. Indeed, structural relaxations (Jahn-Teller–like distortions) and electronic self-consistency ensure that charge transfer is minimized. All atoms are practically neutral and experiments detect only a minor charge oscillation [9,27]. X-ray absorption and EELS data probe orbital occupancy, not physical charge, so that they establish oxidation-state or orbital-occupancy ordering, not charge ordering.

It is clear that DFT/GGA provides a satisfactory description of the ground-state properties of the CMO system. LSDA + U/GGA + U and other theories of strongly correlated electrons, e.g., DMFT, have been used widely for TM oxides. They often improve agreement with experimental data over LSDA or GGA [28]. For comparison, we performed GGA + U calculations for the CMO system and found that the results for ground-state properties do not agree with experimental data as well as the GGA results. In particular, compared to GGA results, the valence DOS

TABLE I. Mn 3*d* orbital occupancy of the majority spin and magnetic moment μ as obtained by GGA calculations, and the corresponding Mn oxidation states in several Mn oxides.

	Mn 3*d* majority-spin occupancy					$\mu(\mu_B)$	Mn formal oxid. state
$CaMnO_3$	0.93	0.93	0.93	**0.46**	0.46	2.6	**+4**
MnO_2	0.95	0.93	0.92	**0.49**	0.47	2.7	**+4**
$LaMnO_3$	0.94	0.93	0.92	**0.88**	0.52	3.3	**+3**
Mn_2O_3	0.93	0.93	0.92	**0.91**	0.46	3.5	**+3**
$CaMnO_3 + 0.33e^-$	0.94	0.94	0.93	**0.56**	0.49	2.8	**+4**
	0.94	0.93	0.93	**0.60**	0.45	2.8	**+4**
	0.94	0.93	0.93	**0.69**	0.45	3.0	**+3**
$CaMnO_3 + 0.50e^-$	0.94	0.94	0.93	**0.59**	0.52	2.9	**+4**
	0.94	0.93	0.93	**0.76**	0.44	3.1	**+3**

from GGA + U have larger bandwidth energies, in disagreement with photoemission data (Fig. 1). The predicted magnetic ordering obtained from GGA + U for CMO at 0, 33%, and 50% doping is shown in Fig. 2 for two different values of U. Clearly, U pushes the crossing point farther away from the experimental value.

The present results call for an assessment of systematic DFT/GGA benchmarks and the extent of discrepancies. For example, viewed by themselves, DFT/GGA results for ordered $La_{0.5}Ca_{0.5}MnO_3$ [blue (or dark gray) circles in Fig. 2] might be interpreted as a failure to predict the observed magnetic ordering (in the data AF prevails up to $x = 0.52$). However, when viewed as a trend with doping, as in Fig. 2, the agreement with experiment is excellent (note the meV scale). It has been believed that one must include double exchange and superexchange explicitly, as a manifestation of strong correlations, to account for the observed magnetic ordering in $La_{0.5}Ca_{0.5}MnO_3$ [29]. Clearly, these effects are included adequately by DFT/GGA. Another example is $LaMnO_3$, for which GGA obtains the correct crystallographic symmetry, but predicts FM ordering instead of the observed AF ordering. The problem can be traced to slightly smaller Jahn-Teller distortions than observed (see, e.g., Refs. [15,30]). However, AF ordering is predicted if the measured distortions are used. Thus, in this case, the magnetic ordering is within the error of DFT/LSDA for atomic positions. GGA + U gets the correct structure (larger Jahn-Teller distortions than GGA) and magnetic ordering.

Overall, we conclude the following. When one examines structural, electronic, and magnetic ground-state properties of the entire LCMO system as opposed to isolated cases, the discrepancies between GGA results and experimental data are small, just as they are in sp-bonded materials, obviating the need to invoke strong correlations. Though it is desirable to have theories that go beyond GGA even for ground-state properties, the task is very challenging because such theories would seek improved performance on the scale of 0.1 eV in total energies and 0.1 Å in bond lengths. Our results demonstrate that, as formulated, GGA + U does not meet this challenge in a key mixed-valence system, even though it is often a clear winner over GGA in isolated cases in other systems. It is clear that systematic DFT/GGA benchmarks are needed for ground-state properties of other systems as well before strong correlations are invoked.

GGA + U and DMFT are usually invoked to account for the observed energy gaps of transition-metal oxides, following the suggestion by Mott for NiO [31] and by Hubbard [32]. In sp-bonded materials, energy gaps are generally calculated with the *GW* scheme [33], which yield satisfactory agreement with data, even in cases where the LDA gap is zero. In recent years, the *GW* scheme has been shown to yield excellent band gaps for TM oxides as well, in particular, for the benchmark case of NiO [34]. This result, together with the results of the present Letter, clearly suggest that systematic and accurate benchmarks using DFT/GGA and by *GW* as an extension for energy gaps are needed to establish any discrepancies from experimental data that need to be addressed by theories that include additional correlations.

We thank E. Dagotto, A. J. Millis, and K. Terakura for valuable comments. Research sponsored in part by the DOE Office of Basic Energy Sciences, Division of Materials Sciences and Engineering, and by the McMinn Endowment at Vanderbilt University. Computations were performed at the National Energy Research Scientific Computing Center.

[1] Y. Murakami *et al.*, Phys. Rev. Lett. **80**, 1932 (1998).
[2] T. Akao *et al.*, Phys. Rev. Lett. **91**, 156405 (2003).
[3] P. G. Radaelli *et al.*, Phys. Rev. B **55**, 3015 (1997).
[4] K. Nakamura *et al.*, Phys. Rev. B **60**, 2425 (1999).
[5] E. Dagotto *et al.*, Phys. Rep. **344**, 1 (2001).
[6] J. García *et al.*, J. Phys. Condens. Matter **13**, 3229 (2001).
[7] J. García *et al.*, J. Synchrotron Radiat. **8**, 895 (2001).
[8] S. Grenier *et al.*, Phys. Rev. B **69**, 134419 (2004).
[9] J. C. Loudon *et al.*, Phys. Rev. Lett. **94**, 097202 (2005).
[10] M. Coey, Nature (London) **430**, 155 (2004).
[11] P. Hohenberg and W. Kohn, Phys. Rev. **136**, B864 (1964).
[12] W. Kohn and L. J. Sham, Phys. Rev. **140**, A1133 (1965).
[13] V. I. Anisimov *et al.*, Phys. Rev. B **44**, 943 (1991).
[14] A. Georges *et al.*, Rev. Mod. Phys. **68**, 13 (1996).
[15] P. Mahadevan *et al.*, Phys. Rev. Lett. **87**, 066404 (2001).
[16] Z. Popovic and S. Satpathy, Phys. Rev. Lett. **88**, 197201 (2002).
[17] M. J. Calderon *et al.*, Phys. Rev. B **68**, 100401 (2003).
[18] V. I. Anisimov *et al.*, Phys. Rev. B **55**, 15 494 (1997).
[19] J. Wang, W. Y. Zhang, and D. Y. Xing, J. Phys. Condens. Matter **14**, 4659 (2002).
[20] M. Varela *et al.*, Annu. Rev. Mater. Res. **35**, 539 (2005).
[21] G. Kresse and J. Furthmüller, Phys. Rev. B **54**, 11 169 (1996).
[22] P. E. Blöchl, Phys. Rev. B **50**, 17 953 (1994).
[23] I. S. Elfimov *et al.*, Phys. Rev. Lett. **82**, 4264 (1999).
[24] P. G. Radaelli *et al.*, Phys. Rev. B **59**, 14 440 (1999).
[25] R. F. W. Bader, *Atoms in Molecules: A Quantum Theory* (Oxford University Press, Oxford, 1990).
[26] R. S. Mulliken, J. Chem. Phys. **23**, 1833 (1955).
[27] J. M. Zuo *et al.*, Nature (London) **401**, 49 (1999).
[28] E. Pavarini *et al.*, Phys. Rev. Lett. **92**, 176403 (2004).
[29] I. Solovyev and K. Terakura, Phys. Rev. Lett. **83**, 2825 (1999).
[30] H. Sawada *et al.*, Phys. Rev. B **56**, 12 154 (1997).
[31] N. F. Mott, Proc. Phys. Soc. London, Sect. A **62**, 416 (1949).
[32] J. Hubbard, Proc. R. Soc. A **276**, 238 (1963).
[33] M. S. Hybertsen and S. G. Louie, Phys. Rev. B **34**, 5390 (1986).
[34] J. L. Li, G. M. Rignanese, and S. G. Louie, Phys. Rev. B **71**, 193102 (2005).
[35] J.-H. Park *et al.*, Phys. Rev. Lett. **76**, 4215 (1996).